Table 2. Structural data for calcite and some U-bearing compounds. M, metal.

Compound	Shell	*N*	*R* (Å)	Mean *R* of M-O (Å)
Calcite (*5*)	Ca-O	6	2.36	2.36
	Ca-C	6	3.21	
	Ca-Ca	6	4.04	
	Ca-Ca	6	4.99	
Brannerite (UTi_2O_6) (*10*)	U-O	6	2.28	2.42
	U-O	2	2.82	
Calciobetafite $[Ca_2(Nb,Ti)_2(O,OH)_7]$ (*11*)	U-O	2	2.23	2.49
	U-O	6	2.58	
Coffinite ($USiO_4$) (*9*)	U-O	4	2.32	2.42
	U-O	4	2.51	
	U-U	4	3.83	
Uraninite (UO_2) (*8*)	U-O	8	2.36	2.36
	U-U	12	3.85	
Uranyl compounds (*12*)	U-O	2	~1.8	2.1–2.3*
	U-O	4–6	2.3–2.5	

*Dependent on grouping.

tion was limited by uraninite solubility [$\sim 10^{-9.47}$ m at pH = 4 to 10, temperature 100 to 300°C (*19*)], we estimate that the distribution ratio $U^{4+}_{calcite}/U^{4+}_{fluid}$ had a range of about 60 to 430 ml/g. There is no evidence that U is segregated into separate U-bearing mineral inclusions (for example, uraninite grains) at this scale, in a manner analogous to the partial segregation of Sr into strontianite within aragonite coral skeletons (*20*).

The sequestration of U^{4+} in the calcite structure explains the anomalously high concentrations of U observed in calcite from reducing environments (*21*) and thus provides insight into the geochemical cycle of U in deep groundwater aquifers and anoxic lacustrine and marine basins. The incorporation of U into calcite as U^{4+} gives a potentially stable host for dispersed U over geological time scales.

References and Notes

1. K. R. Ludwig *et al.*, *Science* **258**, 284 (1992); J. C. Brannon *et al.*, *ibid.* **271**, 491 (1996).
2. A. D. Russell, S. Emerson, B. K. Nelson, J. Erez, D. W. Lea, *Geochim. Cosmochim. Acta* **58**, 671 (1994).
3. P. Zeh, K. R. Czerwinski, J. I. Kim. *Radiochim. Acta* **76**, 37 (1996).
4. D. Langmuir, *Geochim. Cosmochim. Acta* **42**, 547 (1978).
5. R. J. Reeder, in *Carbonates: Mineralogy and Chemistry*, vol. 23 of *Reviews in Mineralogy*, R. J. Reeder, Ed. (Mineralogical Society of America, Washington, DC, 1983), pp. 1–47.
6. J. C. Brannon, F. A. Podosek, S. C. Cole, in *Soc. Econ. Geol. Spec. Publ. 4* (1996), pp. 536–545.
7. X-ray absorption measurements were made using wiggler beamline 4-3 at the Stanford Synchrotron Radiation Laboratory (SSRL). The energy of the incident beam (1 by 10 mm) was selected by a Si (220) monochromator, detuned to ~50% intensity for harmonic rejection. Measurements were made in fluorescence mode at the U L_2 edge (20,948 eV); interference from Sr K-edge fluorescence precluded U fluorescence measurements at the U L_3 edge. The powdered sample (~0.5 g) was held with Kapton tape in a slotted Al plate. This plate was held at 10 K in a continuous-flow liquid He cryostat for the 20-hour duration (25 scans) of the measurements. The U $L_{\beta 1}$ fluorescence at 17,220 eV was monitored continuously with a 13-element Ge detector. X-ray absorption data were analyzed with the EXAFSPAK code (*22*). Curve fitting was performed with single-scattering theoretical phase and amplitude functions obtained from the program FEFF 6.01a (*23*). X-ray fluorescence mapping of U was done with white, bending-magnet radiation at beamline X26A at the National Synchrotron Light Source (*24*). A 1-mm² area of calcite was examined with a 10-μm by 10-μm beam spot size. A 50-μm² grid spacing was used to approximately match the U fluorescence sampling depth, with 30 s of data acquisition per pixel. The U concentration reference was National Institute of Standards and Technology standard reference material 612 (37 ppm of U in a glass matrix).
8. B. Wasserstein, *Nature* **174**, 1004 (1954).
9. L. H. Fuchs and E. Gebert, *Am. Mineral.* **43**, 243 (1958).
10. J. T. Szymanski and J. D. Scott, *Can. Mineral.* **20**, 272 (1982).
11. F. Mazzi and R. Munno, *Am. Mineral.* **68**, 2262 (1983).
12. P. C. Burns, M. L. Miller, R. C. Ewing, *Can. Mineral.* **34**, 845 (1996); H. A. Thompson, G. E. Brown Jr., G. A. Parks, *Am. Mineral.* **82**, 483 (1997).
13. R. Shannon, *Acta Crystallogr.* **32**, 751 (1976).
14. G. M. Lamble, R. J. Reeder, P. A. Northrup, *J. Phys. IV* **7**, C2793 (1997).
15. M. Ishikawa and M. Ichikuni, *Chem. Geol.* **42**, 137 (1984); E. Busenberg and L. N. Plummer, *Geochim. Cosmochim. Acta* **49**, 713 (1985).
16. J. F. Gratz and K. C. Misra, *Econ. Geol.* **82**, 1790 (1987); K. C. Misra and C. Lu, *Eur. J. Mineral.* **4**, 977 (1992).
17. J. L. Banner, G. J. Wasserburg, J. H. Chen, C. H. Moore, *Earth Planet. Sci. Lett.* **101**, 296 (1990): J. G. Zukin, D. E. Hammond, T. L. Ku, W. A. Elders, *Geochim. Cosmochim. Acta* **51**, 2719 (1987).
18. D. E. Meece and J. K. Benninger, *Geochim. Cosmochim. Acta* **57**, 1447 (1993).
19. G. A. Park and D. C. Pohl, *ibid.* **52**, 863 (1988).
20. R. B. Greegor, N. E. Pingitore Jr., F. W. Lytle, *Science* **275**, 1452 (1997).
21. C. Israelson, A. N. Halliday, B. Buchardt, *Earth Planet. Sci. Lett.* **141**, 153 (1996).
22. G. N. George and I. J. Pickering, *EXAFSPAK: A Suite of Computer Programs for Analysis of X-ray Absorption Spectra* (SSRL, Stanford, CA, 1995).
23. J. J. Rehr, J. Mustre de Leon, S. I. Zabinsky, R. C. Alberts, *J. Am. Chem. Soc.* **113**, 5135 (1991); J. Mustre de Leon, J. J. Rehr, S. I. Zabinsky, R. C. Albers, *Phys. Rev. B* **44**, 4146 (1991).
24. S. R. Sutton, M. L. Rivers, S. Bajt, K. W. Jones, *Nucl. Instrum. Methods Phys. Res. Sect. B* **75**, 5533 (1993); J. V. Smith and M. L. Rivers, in *Microprobe Techniques in the Earth Sciences*, P. J. Potts, J. F. W. Bowles, S. J. B. Reed, M. R. Cave, Eds. (Chapman & Hall, London, 1995), pp. 163–233.
25. This work was supported by the Geosciences and Chemical Sciences subprograms of the Office of Basic Energy Sciences, U.S. Department of Energy. We thank P. de Cecco (SSRL) for assistance with EXAFS measurements.

9 March 1998; accepted 4 June 1998

Coaxial Nanocable: Silicon Carbide and Silicon Oxide Sheathed with Boron Nitride and Carbon

Y. Zhang,* K. Suenaga, C. Colliex, S. Iijima

Multielement nanotubes comprising multiple phases, with diameters of a few tens of nanometers and lengths up to 50 micrometers, were successfully synthesized by means of reactive laser ablation. The experimentally determined structure consists of a β-phase silicon carbide core, an amorphous silicon oxide intermediate layer, and graphitic outer shells made of boron nitride and carbon layers separated in the radial direction. The structure resembles a coaxial nanocable with a semiconductor-insulator-metal (or semiconductor-insulator-semiconductor) geometry and suggests applications in nanoscale electronic devices that take advantage of this self-organization mechanism for multielement nanotube formation.

The discovery of pure carbon nanotubes (*1*) has resulted in extensive investigations to realize heteroatomic nanotubes; BN nanotubes (*2*) and the nanotubes in the B-C-N ternary system (*3–5*) have been reported so far. The electronic structure of such an individual tube can be controlled by its chemistry (*6*), whereas that of a pure carbon nanotube is controlled by the chirality and diameter (*7*). By combining the different types of nanotubes in axial or radial direction, nanoscaled electronic devices with a variety of functions may be realized (*4, 5, 8*). Progress has also been made in fabricating solid nanowires by

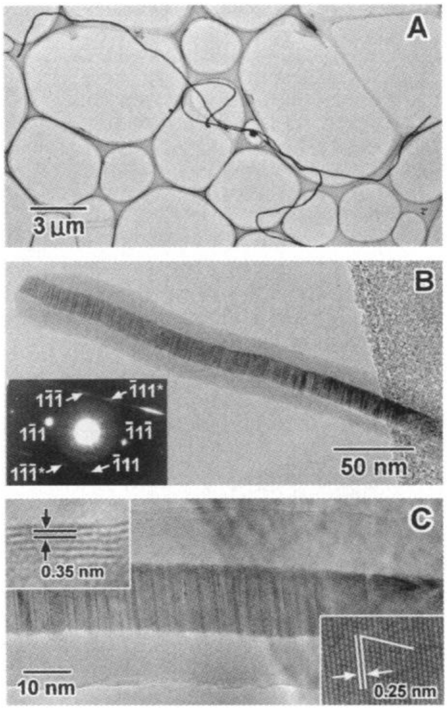

Fig. 1. (**A**) A low-magnification transmission electron micrograph of nanocables. (**B**) A magnified image shows a crystalline core and an amorphous layer. (**Inset**) The selected area diffraction pattern indicates that the crystalline core is β-phase SiC with the <110> axis parallel to the electron beam. The asterisks represent twinning planes. (**C**) A high-resolution image of the nanocable structure. (**Top inset**) The magnified lattice fringes of the outer C-BN layers. (**Bottom inset**) A magnified lattice image of the β-phase SiC core.

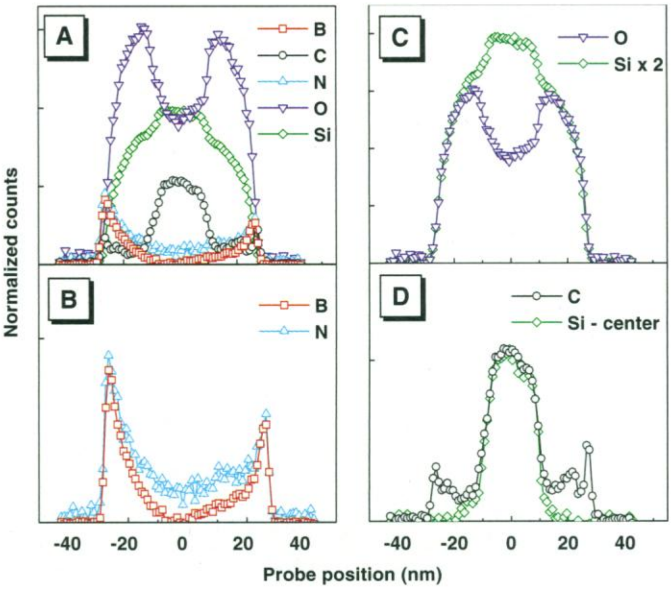

Fig. 2. Elemental profiles across a nanocable. (**A**) Profiles of all of the elements present in the nanocable. (**B**) The B and N profiles showing the tubular feature of the outer sheath and unity atomic ratio (*17*). (**C**) The Si and O profiles, in which the Si concentration is doubled to compare it with that of O; the Si:O ratio in the intermediate layer is shown to be 1:2. (**D**) A reduced profile of Si in the center core, obtained by subtracting the contribution of Si comprised in the SiO_2 layer from the total Si concentration, is compared with the C profile. The Si:C ratio in the core wire is unity.

filling the hollow cavity of the nanotubes with elements or compounds (*9*) and nanorods through a carbon nanotube–confined reaction (*10*). Relatively long nanowires encapsulated in carbon nanotubes have also been synthesized with the arc-discharge method (*11*).

Here we demonstrate a coaxial structure that combines the silicon-based nanowires with the graphitic B-C-N nanotubes in the radial direction and also infer a nanoscale self-organization mechanism for the nanotube formation consisting of multiple phases. The laser ablation setup formerly used for B-C-N nanotube synthesis (*4*) was modified to produce the coaxial nanowire with the B-C-N sheath. We used a mixed and compressed powder of BN, C, SiO, and Li_3N as starting materials (*12*). Wirelike materials obtained in the ablated products are shown in a transmission electron micrograph (Fig. 1A) (*13*). The wires are quite clean with very few particles attached to their surface. They have high aspect ratios with lengths of up to several tens of micrometers and diameters of a few tens of nanometers. The diameter is relatively homogeneous for each wire. A magnified image in Fig. 1B shows that the wire has a crystalline core and a surrounding amorphous layer (*14*). The selected area diffraction pattern (inset in Fig. 1B) indicates that the crystalline core is β-phase SiC, with the <110> axis parallel to the electron beam. Diffraction spots from {111} planes were labeled, with asterisks representing twinning planes. The existence of stacking faults implies that the SiC core was formed through a solid-gas reaction of C and SiO (*15*). In a high-resolution image (Fig. 1C), we can see an additional graphitic sheath outside the amorphous layer (*14*). Lattice fringes from the sheath (top left inset of Fig. 1C) indicate that the interlayer distance is ~0.35 nm, near the (002) spacing of turbostratic graphitic layers of BN or C. From the crystalline SiC core (bottom right inset of Fig. 1C), we can see the typical <110> projection of a face-centered cubic structure with (111) plane spacing of ~0.25 nm. The structure shown here is similar to that of a coaxial cable conventionally used in signal transmission, so we call it a coaxial nanocable.

Elemental profiles across a nanocable were obtained by scanning a finely focused electron probe and recording the energy-loss spectra (*16*). The K edge weights were normalized for chemical profiling of all of the elements except for silicon for which the L edge was used; therefore, the profiles represent the distribution of atomic concentrations (*16*, *17*). The profiles of B, N, and O show two peaks with a central hollow, featuring tubular geometry due to projection of cylindrical distribution (Fig. 2A). The inner diameters of the B and N profiles are close to the outer diameters of the Si and O profiles. In Fig. 2B, the atomic ratio of B and N is near unity (*18*), which suggests that B and N form the stoichiometric BN. The Si:O ratio is very near 1:2 at the amorphous region between the crystallized core and the graphitic sheath (Fig. 2C), which indicates that the intermediate layer is amorphous SiO_2. By subtracting the contribution of Si comprised in the intermediate layer, which is equivalent to half of the O contribution, we can reveal the Si profile contributed from the crystallized core (Fig. 2D). The profile of C is also composed of two parts, one from the center core and the other from the thin outer tubular layer. The equiatomic correlation between C and Si at the center core

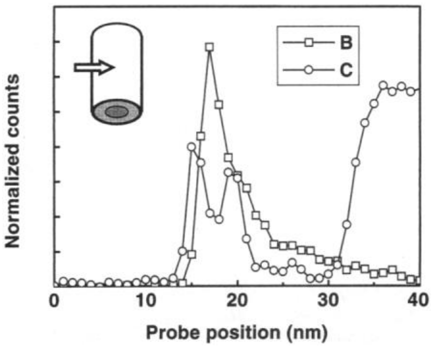

Fig. 3. Profiles of B and C across half of a nanocable, showing a phase separation of graphite and BN layers.

Y. Zhang, Fundamental Research Laboratories, NEC Corporation, 34 Miyukigaoka, Tsukuba, Ibaraki 305-8501, Japan. K. Suenaga, Laboratoire de Physique des Solides, URA 002, Université de Paris-Sud, Bâtiment 510, 91405 Orsay, France, and Japan Science and Technology, Department of Physics, Meijo University, Nagoya 468-8502, Japan. C. Colliex, Laboratoire de Physique des Solides, URA 002, Université de Paris-Sud, Bâtiment 510, 91405 Orsay, France. S. Iijima, Fundamental Research Laboratories, NEC Corporation, 34 Miyukigaoka, Tsukuba, Ibaraki 305-8501, Japan, and Japan Science and Technology, Department of Physics, Meijo University, Nagoya 468-8502, Japan.

*To whom correspondence should be addressed. E-mail: zhang@frl.cl.nec.co.jp

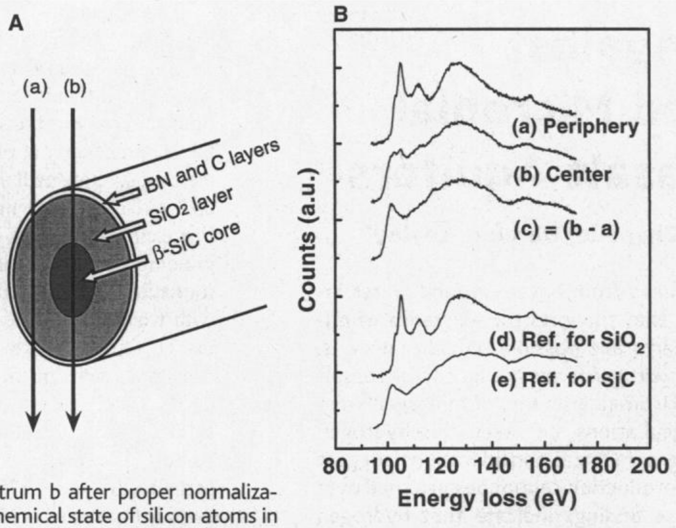

Fig. 4. (**A**) A schematic illustration of a multiphase nanocable. Solid arrows indicate the probe positions in the electron energy-loss fine structure analysis. (**B**) Silicon L edge fine structures obtained from the peripheral layer (spectrum a) and the center region (spectrum b) of a nanocable as shown in (A). Spectrum b contains the contribution from both the center core and the amorphous layer. Spectrum c was obtained by subtracting spectrum a from spectrum b after proper normalization, so it represents the chemical state of silicon atoms in the core wire. By comparing spectra a and c with the reference spectra d and e (*18*), an amorphous SiO_2 phase and a crystalline β-phase SiC are confirmed for the intermediate layer and the core, respectively; a.u., arbitrary units.

confirms that the crystalline core is a stoichiometric SiC. In a detailed study of B and C profiles from the graphitic sheath (Fig. 3), we noticed an anticorrelation between the B and C profiles, which indicates the atomically immiscible BN and C as previously reported on the arc-discharged BCN products (*5*).

Different bonding states of Si atoms within the nanocable were verified by the fine structure analysis of their absorption edges. The Si L edges from the amorphous region (spectrum a) and the core region (spectrum c) are compared in Fig. 4B. The latter was obtained by subtracting spectrum a from spectrum b after proper normalization, because spectrum b contains the contribution from both the core and the amorphous layer (see Fig. 4A). Features seen in the near-edge region (up to 160-eV loss) reflect the electronic states and coordination of the Si atoms (*17*). The spectra obtained from the nanocable (a and c) show good agreement with the reference spectra obtained from the single phase of SiO_2 (d) and SiC (e) (*19*). The anomalous core level shift, about 6 eV higher in the peripheral SiO_2 layer, is due to charge transfer from Si to O. Therefore, we can assign, by the chemical states, the SiC to the core wire and the SiO_2 to the intermediate amorphous layer.

The experimentally determined structure of nanocable promises great potential in applications for electronic transportation or nanodevices because it has the one-dimensional features of both nanowire and nanotube in the axial direction and builds an ideal semiconductor-insulator-semiconductor (or semiconductor-insulator-metal) heterojunction in the radial direction (*20*). The importance of the nanocable is not only the superior structure itself but also the control of the structure formation. The growth of nanocables could be divided into two steps. The first is the formation of SiC-SiO_2 nanowire through a reaction C (solid or vapor) + 2SiO (gas) → SiC (solid) + SiO_2 (solid) (*10*, *15*). The second step is the coating of the BCN sheath, with the phase separation of BN and C into nanodomains. Although Li was not detected inside the nanocable, we found that it played a crucial role in forming the graphitic sheath. Without Li_3N in the starting materials, only SiC-SiO_2 wires were formed without any graphitic sheath. This result is not surprising because tubular BN layers are difficult to form without a graphite template (*4*), whereas C reacts easily with SiO at the experimental temperature. The high amount of activity of Li with SiO could be the reason why the outer C layers could survive. Moreover, Li is able to accelerate the formation of graphitelike BN (*21*). Although many details are still unknown, we can see that the phases formed in the two steps are all controlled by the chemical reactions. Under the same scenario, self-organization of nanocables with different components is also possible by changing chemicals in starting materials. The electronic properties of the nanocable can, therefore, be tailored by combining different nanowires and nanotubes.

References and Notes

1. S. Iijima, *Nature* **354**, 56 (1991); S. Iijima and T. Ichihashi, *ibid.* **363**, 603 (1993).
2. N. G. Chopra *et al.*, *Science* **269**, 966 (1995); A. Loiseau, F. Willaime, N. Demoncy, G. Hug, H. Pascard, *Phys. Rev. Lett.* **76**, 4737 (1996); M. Terrones *et al.*, *Chem. Phys. Lett.* **259**, 568 (1996); D. Golberg *et al.*, *Appl. Phys. Lett.* **69**, 2045 (1996).
3. O. Stephan *et al.*, *Science* **266**, 1683 (1994); Z. Weng-Sieh *et al.*, *Phys. Rev. B* **51**, 11229 (1995); P. Redich *et al.*, *Chem. Phys. Lett.* **260**, 465 (1996); M. Terrones *et al.*, *ibid.* **257**, 576 (1996).
4. Y. Zhang, H. Gu, K. Suenaga, S. Iijima, *Chem. Phys. Lett.* **279**, 264 (1997).
5. K. Suenaga *et al.*, *Science* **278**, 653 (1997).
6. A. Rubio, J. L. Corkill, M. L. Cohen, *Phys. Rev. B* **49**, 5081 (1994); X. Blase, A. Rubio, S. G. Louie, M. L. Cohen, *Europhys. Lett.* **28**, 335 (1994); Y. Miyamoto, A. Rubio, M. L. Cohen, S. G. Louie, *Phys. Rev. B* **50**, 4976 (1994); Y. Miyamoto, A. Rubio, S. G. Louie, M. L. Cohen, *ibid.*, p. 18360; X. Blase, J.-C. Charlier, A. De Vita, R. Car, *Appl. Phys. Lett.* **70**, 197 (1997).
7. M. S. Dresselhaus, G. Dresselhaus, P. Eklund, *Science of Fullerenes and Carbon Nanotubes* (Academic Press, New York, 1996). Experimental verification with scanning tunneling microscope has been reported recently by J. W. G. Wildöer, L. C. Venema, A. G. Rinzler, R. E. Smalley, and C. Dekker [*Nature* **391**, 59 (1998)] and T. W. Odom, J.-L. Huang, P. Kim, and C. M. Lieber [*ibid.*, p. 62].
8. M. Dresselhaus, *Physics World* (May 1996), p. 18.
9. P. M. Ajayan and S. Iijima, *Nature* **361**, 333 (1993); P. M. Ajayan *et al.*, *ibid.* **362**, 522 (1993); S. C. Tsang, Y. K. Chen, P. J. F. Harris, M. L. H. Green, *ibid.* **372**, 159 (1994); D. Ugarte, A. Châtelain, W. A. de Heer, *Science* **274**, 1897 (1996).
10. H. Dia, E. W. Wong, Y. Z. Lu, S. Fan, C. Lieber, *Nature* **375**, 769 (1995); D. Zhou and S. Seraphin, *Chem. Phys. Lett.* **222**, 233 (1994); W. Han *et al.*, *ibid.* **265**, 374 (1997); W. Han, S. Fan, Q. Li, Y. Hu, *Science* **277**, 1287 (1997).
11. S. Seraphin, D. Zhou, J. Jiao, J. C. Withers, R. Loutfy, *Nature* **362**, 503 (1993); C. Guerret-Piécourt, Y. Le Bouar, A. Loiseau, H. Pascard, *ibid.* **372**, 761 (1994); A. Loiseau and H. Pascard, *Chem. Phys. Lett.* **256**, 246 (1996).
12. In the experiment, the secondary harmonics beam (wavelength of 532 nm) from a pulsed Nd:yttrium-aluminum-garnet laser (Qanta-Ray GCR-200; Spectra-Physics, Mountain View, CA) was focused on the target surface to get an energy density of about 3 J/cm^2 per shot. The target was placed at the center of a quartz reactor tube heated to 1200°C. The flow rate of nitrogen carrier gas was 300 standard cubic centimeters per minute, and the system pressure was 500 torr. At high temperature, SiO vapor can be produced by a reaction between Li^+ ions and the quartz tube during laser ablation. Thus, we could still obtain a similar result using a target without SiO powder. We also found that the result is not sensitive to the concentration of carbon in the target.
13. Microscopic observation was performed with a high-resolution transmission electron microscope (Topcon 002B) working at 200 kV.
14. Although the diameter is homogeneous throughout a wire, the size distribution is diverse among different wires. The core has a lateral dimension in the same order with the thickness of the amorphous layer, which varies from 3 to 20 nm, depending on the diameter of the wire. The outer graphitic sheath usually contains 4 to 15 shells, which are 1.4 to 5.1 nm in thickness, independent of the wire diameter.
15. W.-S. Seo and K. Koumoto, *J. Am. Ceram. Soc.* **79**, 1777 (1996).
16. A scanning transmission electron microscope [VG-HB501 (VG Microscopes, Sussex, England)] working at 100 kV equipped with a parallel energy-loss spectrometer [Gatan (Warrendale, PA) PEELS 666] was used. The spatial resolution was about 0.5 nm. See C. Colliex, *J. Electron Microsc.* **45**, 44 (1996).
17. R. F. Egerton, *Electron Energy-Loss Spectroscopy in the Electron Microscope* (Plenum, New York, ed. 2, 1996).
18. A slight disaccord between the B and N profiles at the center point is due to the quantification problem of the B K edge spectra. The long tail of L edge from Si present at the center of tubes overlaps the B K edge and affects the background subtraction there.
19. The reference spectra were provided by D. Imhoff and N. Brun.
20. SiC is a large gap (3 eV) semiconductor, SiO_2 and BN tubes are insulating, and carbon nanotubes are metallic or semiconducting (*7*).
21. T. S. Bartnitskaya, V. I. Lyashenko, A. V. Kurdyumov, N. F. Ostroskaya, I. G. Rogovaya, *Powder Metallurgy Metal Ceram.* **33** (nos. 7 to 8), 335 (1994).
22. This work was partially supported by the Special Coordination Funds of the Science and Technology Agency of the Japanese Government and a New Energy and Industrial Technology Development Organization international research grant. The Sumitomo Foundation is acknowledged by K.S.

5 May 1998; accepted 7 July 1998